Electric-field driven translocation of ssDNA through hydrophobic nanopores.

Taylor Haynes,[1] Iain P.S. Smith[1], E. Jayne Wallace[2], Jemma L. Trick[3], Mark S.P. Sansom[4] and Syma Khalid[1]*

[1]School of Chemistry, University of Southampton, Highfield Campus, Southampton, SO17 1BJ, [2]Oxford Nanopore Technologies Ltd, Oxford. [3]Department of Physics, King's College London, London, [4] Department of Biochemistry, University of Oxford, South Parks Road, Oxford OX1 3QU, United Kingdom

Supporting Information Placeholder

ABSTRACT: The accurate sequencing of DNA using nanopores requires control over the speed of DNA translocation through the pores and also of the DNA conformation. Our studies show that ssDNA translocates through hour-glass shaped pores with hydrophobic constriction regions when an electric field is applied. The constriction provides a barrier to translocation and thereby slows down DNA movement through the pore compared to pores without the constriction. We show that ssDNA moves through these hydrophobic pores in an extended conformation, and therefore does not form undesirable secondary structures that may affect the accuracy of partial current blockages for DNA sequencing.

Electric field driven movement of molecules through nanopores embedded within insulating membranes forms the basis of nanopore-based biosensors[1]. Such nanopores may be composed of biological molecules, e.g. engineered membrane proteins or nucleic acids, or they may be synthetic e.g. based on graphene sheets or carbon nanotubes. These nanopores have been used for applications ranging from detection of drugs to DNA sequencing. Control over the movement of analyte molecules typically arises from altering the strength of the applied voltage or reducing the dimensions of the pore. However, a more elegant approach, affording better control would be to incorporate gates within the pore that would enable switching of the pore between functionally active and inactive states.

A number of channel and pore proteins are known to contain a hydrophobic region within the lumen of their pore regions[2]. Computational studies have shown that these regions while being sterically 'open'; may still be of sufficient local hydrophobicity that they prevent permeation of both water molecules and small charged species[3-4]. Hydrophobic conically shaped nanopores in polyethylene terephthalate (PET) films have also shown these 'dewetting' properties[5]. Combined experimental and computational studies have demonstrated the existence of hydrophobic barriers to permeation in ion channels, e.g. Aryal et al[6]. Recently a number of pores based on a beta barrel topology were designed to incorporate hydrophobic regions that could be wetted upon application of an electric field, and then de-wet once the field is removed[7].

RESULTS AND DISCUSSION

Model nanopores in an applied electric field. The nanopores studied here mimic a beta barrel protein. Each barrel is composed of 14 antiparallel strands and contains a hydrophobic region near the center giving it an 'hourglass' shape. The central constriction is formed by rings of the following amino acid residues GAVLVAG. Thus the narrowest region of the pore is formed by three rings of bulky hydrophobic amino acids, namely the VLV region.

Trick et al have previously shown that when these pores are placed within a phospholipid bilayer, under equilibrium conditions, the hydrophobic regions remain essentially dry; with a mean water flux of only 0.4 water molecules per ns through the pore[7].

Here we studied the hourglass pore as reported by Trick et al[4] and also two modifications of this pore. In the first modification, the ring of TRP residues present at the mouths of the original pore were mutated to TYR to explore any differences in the pore behavior as a function of the anchoring aromatic residues. In the second modification, the rings of hydrophobic sidechains forming the hydrophobic constriction region, VLV, were replaced by GGG, to give a wider pore (radius of ~0.8 nm compared to 0.5 with the constriction) with a cylindrical topology. We refer to this second modified pore as the 'reference pore'.

We explored the behavior of the pores under an applied electric field. The dimensions of the pores fluctuate only

by a small amount under an applied electric field of 0.2 Vnm^{-1}, showing the pores are stable and resilient under these conditions (supplementary information). The radius at the constriction region, which is composed of two bands of valine residues, is about 0.4 nm in both pores. As expected, under an applied field the pores wetted; the mean bi-directional water fluxes through the original pore and the TYR-mutant are 61 ns^{-1} (±16) and 61 ns^{-1} (±23) respectively. The TRP to TYR mutation has no effect on the water flux of the open pore, furthermore in the results that follow, there is also no difference in behavior of DNA within the two sets of pores, therefore the data for 'hour-glass' pore includes both sets of pores. The water flux for the reference pore is 69 ns^{-1} (±23).

DNA translocation under an applied electric field

The translocation of ssDNA through these pores was investigated. A 16-nucleotide strand of DNA with sequence 5'ATATCGCGATATCGCG-3' was positioned with the 5' end nearest to the mouth of the pores. Two different initial distances from the pore were investigated; (1) the DNA terminal base is initially located at the mouth of the pore (2) the DNA is threaded through the pore, with the terminal nucleotide located beyond the two rings of valine residues (Figure 1). In three control simulations without an applied electric field, the DNA was observed to coil around the mouth of the pore, interacting with the aromatic residues (supplementary information). As expected, DNA did not enter the pore, given it is highly charged and the pore has a hydrophobic interior. Thus the electric field acts as a switch for wetting the pores and driving the entry of DNA.

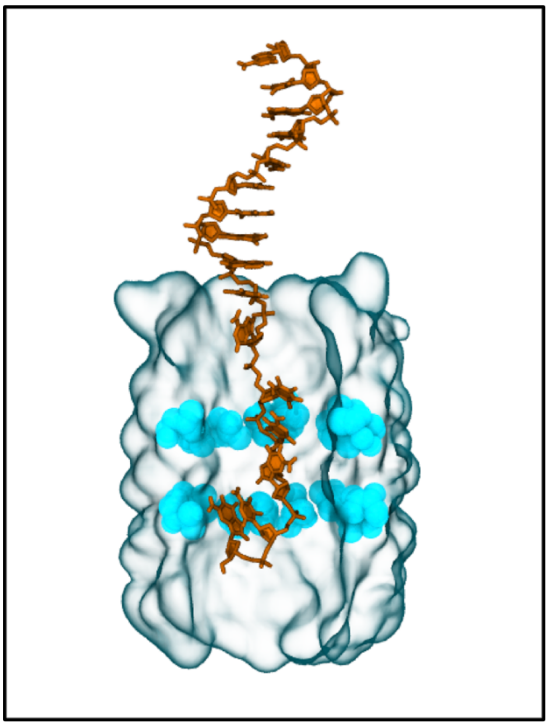

Figure 1: Initial location of ssDNA that is pre-threaded through the entrance of the pore and the constriction region. The valine residues are shown in cyan, DNA is orange.

At a field strength of 0.2 V nm^{-1}, in six independent simulations of the reference pore when DNA was not pre-threaded into the pore, DNA remained associated with the pore entrance in five of the simulations, and only entered the pore once. In contrast, in six independent simulations of the reference pore when DNA was pre-threaded through the pore entrance, full DNA translocation was observed within 10 ns in each simulation. This indicates that there is no appreciable barrier to DNA translocation once the terminal nucleotides have moved beyond the pore entrance. Three simulations of the DNA pre-threaded through the reference pore at the lower strength of 0.1 V nm^{-1}, did not show any translocation even when the simulation were extended to 30 ns. For the hourglass shape pores, a total of 36 independent simulations were performed. A summary of the DNA locations at the start and end of the simulations is provided in table 1.

Table 1 A summary of the DNA translocation behavior as a function of its starting position relative to the entrance of the pore. The values in parenthesis correspond to simulations with a field strength of 0.1 Vnm^{-1}, with all others at 0.2 Vnm^{-1}. A breakdown of the behavior of the data for the hourglass pores for the TRP and TYR pores separately is provided in the supplementary information.

Initial DNA location		Final DNA location (number of simulations)		
		DNA at entrance	DNA at constriction/or inside pore	Translocation through pore
Hour glass pores	Threaded through pore constriction	0	(3)	9
	At pore entrance	8 (2)	6 (1)	7
Reference pores	Threaded through pore entrance	0	(3)	6
	At pore entrance	6	-	-

In all of our simulations the hour-glass pore remained stable within the electric field and showed expected bi-directional water flux behavior. DNA translocation was only observed at a field strength of 0.2 V nm^{-1} (equivalent to 600 mV across the membrane) on the timescale of the simulations. At the lower field strength, DNA translocation beyond the constriction was not observed at all. This is in agreement with our previously reported work on DNA translocation through pores based on α-hemolysin in

which 600 mV across the membrane mimetic slab was required for translocation[8]. For simulations in which DNA translocation was observed, there was reduced water flux while the DNA was within the pore, but this increased to the rate observed for the unoccupied pore, once the DNA had translocated. Linear regression yields a gradient of 0.06 for the unoccupied pore, corresponding to a flux of ~ 62 ns^{-1}. The gradient corresponds to a 33% reduction in the flux when DNA is within the pore at t = 0-6.2 ns, but then recovers to 0.06 when DNA exits the pore at t > 6.2 ns, in agreement with the value from the simulation in which there is no DNA present. Thus the pore retains its structural integrity throughout the process of translocation (Figure 2). DNA that remained at the entrance of the pore throughout the simulation resulted in reduced water flux compared to the open pore as the simulation proceeded, as the DNA occluded increasing amounts of the pore entrance. While DNA is inside both the reference and hourglass pores, the flux through both pores is remarkably similar (Figure 2).

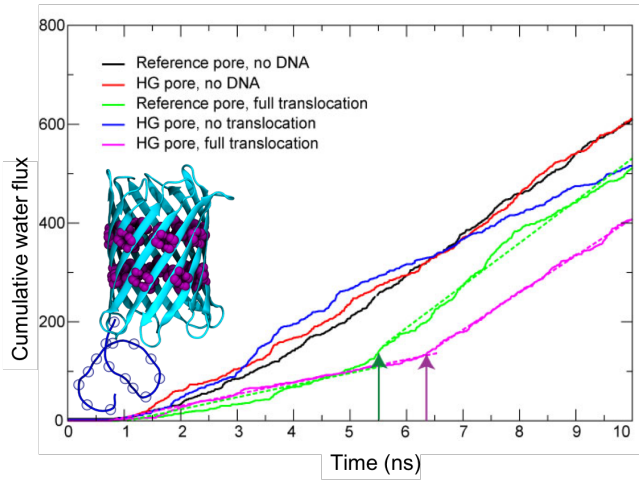

Figure 2: The bidirectional water flux through the hourglass (HG) and reference pores from typical simulations. Dotted lines show the linear regression lines for the cases in which DNA translocation is observed, while the arrows indicate the time at which translocation is complete.

Overall three types of DNA behavior were observed; (1) the DNA remained tethered to the mouth of the pore throughout the simulation, (2) the DNA was able to translocate past the mouth of the pore, but was unable to move past the hydrophobic barrier presented by the valine residues, and (3) the DNA was able to fully translocate through the pore (Figure 3). In all nine simulations in which the DNA was initially threaded through the constriction region, full translocation was observed indicating there are no appreciable barriers to translocation beyond the constriction region, at this field strength. When the DNA was located at the entrance, at the start of the simulation, almost equal occurrences of the three behaviors were observed. In simulations in which the terminal base was able to pass through the entrance of the pore, a subsequent barrier to translocation was encountered at the VLV constriction site. Interestingly even with an electric field of 0.2 Vnm^{-1}, the subtle difference between the motion of the DNA as it moves past valine vs the leucine residues can be discerned (Figure 3). The DNA motion past the bands of valine residues is slower compared to its movement past the leucine residues in-between the two bands of valines. The movement of DNA once past the VLV region, is smooth and unhindered until the pore exit is encountered. This is as expected from our simulations of the reference pore in which the VLV region was replaced by GGG; these pores did not show any barriers to DNA translocation within the pore. The third barrier to translocation in the hour-glass pores is the exit of the pore. In each one of the simulations in which translocation was observed (16/30 simulations at 0.2 Vnm^{-1}), the DNA remained associated with the pore exit to some extent, either coiled around to maximize contact with the short turns of the pore, or tethered by the terminal nucleotide while the rest of the DNA moved away into bulk solution (Figure 3). The DNA remained associated with the pore exit even when this simulation was extended to 100 ns. It is worth mentioning here that extension of more of the simulations beyond 20 ns may lead to untethering of the DNA from the pore exit given the translocation process is stochastic. However we note that the tethering effect is observed despite the electric field applied across the membrane in the simulations being greater (~ 600 mV and 300 mV, as the membrane is approximately 3 nm in width) than that in corresponding experimental studies (120-180 mV)[9]. Thus, our results show that the pore exit is clearly a region through which DNA movement is slower compared to the non-constriction regions of the pore.

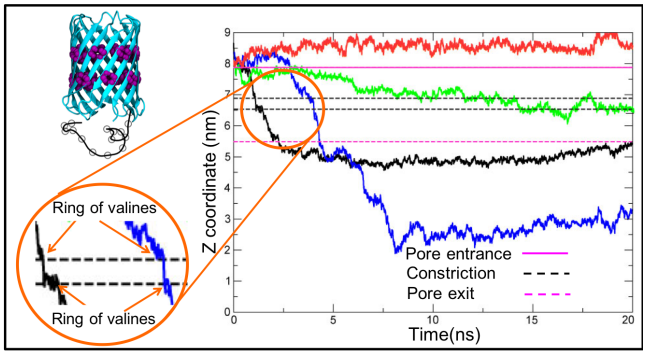

Figure 3: The z coordinate of the leading DNA nucleotide (closest to pore entrance) as a function of time, for scenarios in which DNA remains at the pore entrance (red), the DNA is unable to overcome the barrier at the constriction (green), the DNA translocates fully through the pore but leading nucleotide remains tethered to the exit (black) and the DNA translocates and the leading nucleotides move away from the pore after ~ 6 ns (blue). The inset shows a close up of the latter two curves, in which the DNA movement through the VLV constriction region. The image at the top left shows the DNA position relative to the pore at the end of the simulation corresponding to the black curve on the plot; even

after pore exit the leading nucleotide is associated with the mouth of the pore.

To identify any molecular-level differences between the cases of DNA translocation and those in which the DNA either failed to enter the pore or failed to move beyond the constriction region we examined the DNA conformation and pore-DNA interactions. When DNA translocation was achieved, we observed that the DNA moved through the pore in an extended conformation. In other words we did not observe any coiling or folding of the DNA while it is within the pore, in stark contrast to our previously reported observations for our pore models based on the β-barrel of α-hemolysin, in which in some mutant pores the end-to-end distance of a ssDNA dodecamer was reduced from 3.8 to 2.5 nm whilst inside the pore due to coiling or bending[10]. The DNA end-to-end distances (provided in the supplementary information) shows that in all simulations in which translocation is observed the DNA is in a linear conformation while it is inside the pore, followed by a marked decrease in the end-to-end distance (e.g. decreasing from 6 nm length between the terminal phosphate groups to only 3 nm within just ~2 ns) indicating rapid bending/coiling once the DNA exits the pore. Coiling upon exit occurs as the DNA is still associated with the pore even after exiting, on the timescale of our simulations and thus can interact with itself. Furthermore once past the constriction region the movement of the DNA is smooth, in contrast to the 'binding and sliding' mechanism observed from previously reported studies for many of the mutant pores based on α-hemolysin that were designed to control the speed of DNA translocation[8]. Interestingly, DNA was observed to coil slightly and very transiently within the reference pores, which have a radius that is closer to the constriction region of α-hemolysin (0.8 nm and 0.6 nm respectively). The DNA termini that is the first to enter the pore was able to interact with the interior walls of the pore, but this did not lead to any long-range coiling of the DNA, indeed coiling was restricted to the terminal 2-3 bases and did not cause any tethering of the pore such as that previously reported from our work on α-hemolysin-mimetic pores (Figure 4)[8]. In the reference pores this short-range, transient coiling was observed throughout the pore, whereas in the hourglass pores, the DNA only coiled once having exited the pore. This strongly suggests that the largely extended conformation of the DNA in these hydrophobic pores is a consequence of the chemical nature of the pore interior, and that the constriction region serves to facilitate maintaining the DNA in this conformation.

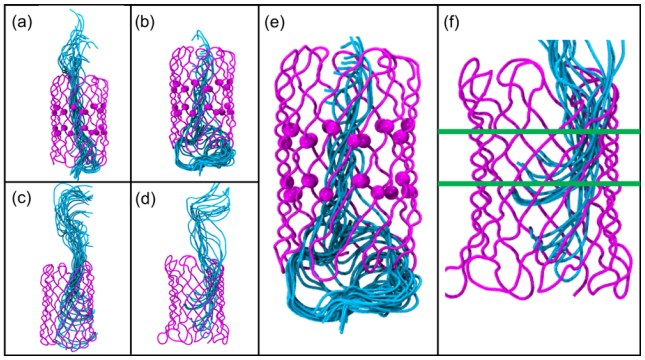

Figure 4: (a) DNA is in a linear conformation while inside the hourglass pores and only coils if (b) one end becomes tethered to the exit of the pore. (c) and (d) In the absence of the constriction transient coiling inside the pore is observed, but this is does not lead to tethering and the DNA is able to translocated through the pore, unhindered. (e) and (f) are close-up views of (b) and (d) respectively. (a)-(d) are independent simulations, in which the DNA backbone is shown at 200 ps intervals while it is in the pore. The magenta spheres represent Ca atoms of the valine residues that form the constriction region in the hourglass pores. In (f) the green lines represent the hypothetical location of the constriction region if this pore was the hourglass rather than the reference.

For the hour-glass shaped pores, in instances in which the DNA remained at the pore entrance throughout the simulation (8/30 simulations at 0.2 Vnm^{-1}), the DNA was observed to interact with the turns connecting the strands of the β-barrel leading to slight narrowing of the pore at the entrance, due to these turns folding into the pore. The DNA formed van der Waals interactions with these turn regions. Unable to move through the pore, but still moving towards the membrane under the influence of the electric field, in these cases, the DNA was observed to interact with the lipid headgroups of the membrane. On the timescale of our simulations this did not lead to any distortion of the membrane. When the DNA is observed to enter the pore but unable to translocate beyond the constriction region, similar DNA-pore interactions are observed. In these simulations, if the nucleotides within the pore are unable to translocate beyond the constriction, before the 'free' nucleotides form interactions with the turns connecting the strands of the pore, leading to the distortion of the latter, the DNA remains anchored within the pore, just above the constriction for the remainder of the simulation.

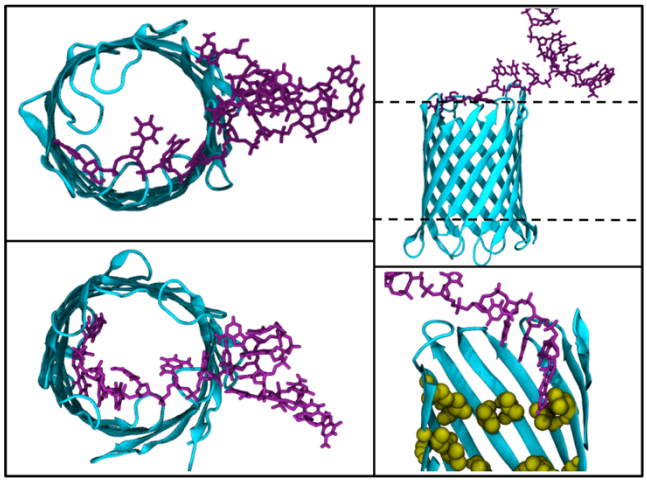

Figure 5: Two simulations in which translocation was not observed; one in which DNA is unable to enter the pore and interacted with the lipid headgroups of the membrane (top left and top right) and one in which the DNA was unable to translocate beyond the constriction region (bottom left and bottom right). Valine residues are shown in yellow in the bottom right panel. The approximate position of lipid headgroups are demarked by the dashed line in the top right panel. All snapshots are shown after 20 ns of simulation.

CONCLUSIONS

In conclusion, our results show that hydrophobic pores originally designed by Trick et al provide the blueprint for a nanopore for DNA sequencing. The speed of DNA translocation is controlled through the hydrophobic constriction region. This region provides a barrier to DNA translocation, and thus slows down the overall translocation rate through the pore, but crucially does not cause any folding of the DNA, this is important as conformational rearrangements in short strands of DNA are likely to impede the accuracy of deciphering partial current blockages for DNA sequencing. We show that while the DNA remains largely linear within hydrophobic pores even in the absence of the constriction region, there is some transient, short-range coiling, although this does not lead to tethering of the DNA inside the pore. When the constriction is present it prevents any coiling at all within the pore. Thus, our simulations show that a hydrophobic constriction within the pore is advantageous over temporary tethering of the DNA with basic amino acids due to the conformational irregularities induced by the latter. To further optimize the pore for translocation, our results suggest that maintaining the DNA in a linear orientation as it goes through the pore entrance is essential as this enables it to overcome the barriers at the pore exit and constriction.

MATERIALS AND METHODS

The hydrophobic gated pore models used in this work were those reported by Trick et al[4]. Where necessary, modifications (e.g. TRP to TYR mutations) were introduced using PyMOL[11]. The ssDNA model used was a 16-nucleotide strand of sequence 5'-ATATCGCGATATCGCG-3', and was generated using the 3DNA package[12].

Simulations were performed using GROMACS versions 5.1.4 and 2016, corresponding to updated package releases, and the GROMOS 53a6 forcefield with Berger lipid definitions[13-15]. Pores were inserted into bilayers of 430 DPPC lipids, solvated using the SPC water model and ions added to a concentration of 1.0 M[16]. Additional ions were added to neutralize systems prior to simulation. Long-range electrostatics were treated using the Particle Mesh Ewald method with a short-range cutoff of 1.4 nm[17]. The van der Waals interactions were truncated at 1.4 nm with long-range dispersion corrections applied to the energy and pressure. During simulation the temperature of the system was maintained at 310 K using the v-rescale thermostat and a coupling constant of 0.1 ps. Pressure was maintained at 1 bar semi-isotropically using the Parrinello-Rahman barostat and a time constant of 1 ps[18]. All bonds were constrained using the LINCS algorithm enabling a timestep of 2 fs[19]. The electric field was imposed by a constant voltage drop across the simulation cell. Periodic boundary conditions were applied in three dimensions as in our own previous work on pores based on α-hemolysin and the work of other groups studying similar phenomena[8, 10, 20-21]. Analysis was conducted using GROMACS utilities and locally written code. Pore radius profiles for the pore models were obtained using HOLE[22]. Water flux counts were obtained by defining xy planes using groups at the pore entrance/exit, and a flux event was only counted once a water molecule had passed across both planes as previously reported by Trick et al[7]. Molecular graphic images were produced using the Visual Molecular Dynamics, VMD package[23].

ASSOCIATED CONTENT

Supporting Information.

The Supporting Information is available free of charge on the ACS Publications website.

PDF file containing a radius profile of the pore under an applied electric field, plot of cumulative water flux, DNA end-to-end distances and plot showing DNA movement with respect to the pore.

AUTHOR INFORMATION

Corresponding Author

S.Khalid@soton.ac.uk

Funding Sources

No competing financial interests have been declared.
TH is funded by Oxford Nanopore Technologies. Calculations were performed on the ARCHER supercomputer through the HECBioSim grant. SK is funded by BBSRC,

EPSRC and MRC. MSPS is funded by BBSRC, EPSRC, The Leverhulme Trust, and Wellcome.

REFERENCES

1. Bayley, H.; Cremer, P. S., Stochastic sensors inspired by biology. *Nature* **2001,** *413* (6852), 226-30.
2. Aryal, P.; Sansom, M. S. P.; Tucker, S. J., Hydrophobic Gating in Ion Channels. *J Mol Biol* **2015,** *427* (1), 121-130.
3. Trick, J. L.; Aryal, P.; Tucker, S. J.; Sansom, M. S., Molecular simulation studies of hydrophobic gating in nanopores and ion channels. *Biochemical Society transactions* **2015,** *43* (2), 146-50.
4. Trick, J. L.; Wallace, E. J.; Bayley, H.; Sansom, M. S., Designing a hydrophobic barrier within biomimetic nanopores. *ACS nano* **2014,** *8* (11), 11268-79.
5. Powell, M. R.; Cleary, L.; Davenport, M.; Shea, K. J.; Siwy, Z. S., Electric-field-induced wetting and dewetting in single hydrophobic nanopores. *Nature nanotechnology* **2011,** *6* (12), 798-802.
6. Aryal, P.; Abd-Wahab, F.; Bucci, G.; Sansom, M. S. P.; Tucker, S. J., A hydrophobic barrier deep within the inner pore of the TWIK-1 K2P potassium channel. *Nature Communications* **2014,** *5*.
7. Trick, J. L.; Song, C.; Wallace, E. J.; Sansom, M. S., Voltage Gating of a Biomimetic Nanopore: Electrowetting of a Hydrophobic Barrier. *ACS nano* **2017,** *11* (2), 1840-1847.
8. Bond, P. J.; Guy, A. T.; Heron, A. J.; Bayley, H.; Khalid, S., Molecular dynamics simulations of DNA within a nanopore: arginine-phosphate tethering and a binding/sliding mechanism for translocation. *Biochemistry* **2011,** *50* (18), 3777-83.
9. Derrington, I. M.; Butler, T. Z.; Collins, M. D.; Manrao, E.; Pavlenok, M.; Niederweis, M.; Gundlach, J. H., Nanopore DNA sequencing with MspA. *Proceedings of the National Academy of Sciences of the United States of America* **2010,** *107* (37), 16060-5.
10. Guy, A. T.; Piggot, T. J.; Khalid, S., Single-stranded DNA within nanopores: conformational dynamics and implications for sequencing; a molecular dynamics simulation study. *Biophys J* **2012,** *103* (5), 1028-36.
11. Schrodinger, L. *The PyMOL Molecular Graphics System, .*
12. Lu, X. J.; Olson, W. K., 3DNA: a software package for the analysis, rebuilding and visualization of three-dimensional nucleic acid structures. *Nucleic Acids Res* **2003,** *31* (17), 5108-21.
13. Pall, S.; Abraham, M. J.; Kutzner, C.; Hess, B.; Lindahl, E., Tackling Exascale Software Challenges in Molecular Dynamics Simulations with GROMACS. *Lect Notes Comput Sc* **2015,** *8759*, 3-27.
14. Oostenbrink, C.; Soares, T. A.; van der Vegt, N. F.; van Gunsteren, W. F., Validation of the 53A6 GROMOS force field. *European biophysics journal : EBJ* **2005,** *34* (4), 273-84.
15. Berger, O.; Edholm, O.; Jahnig, F., Molecular dynamics simulations of a fluid bilayer of dipalmitoylphosphatidycholine at full hydration, constant pressure and constant temperature. *Biophys. J.* **1997,** *72*, 2002-2013.
16. Berweger, C. D.; van Gunsteren, W. F.; Mullerplathe, F., Force-field parametrization by weak-coupling - reengineering SPC water. *Chem. Phys. Lett.* **1995,** *232*, 429-436.
17. Darden, T.; York, D.; Pedersen, L., Particle mesh Ewald - an N.log(N) method for Ewald sums in large systems. *J. Chem. Phys.* **1993,** *98* (12), 10089-10092.
18. Parrinello, M.; Rahman, A., Polymorphic transitions in single-crystals - a new molecular dynamics method. *J. Appl. Phys.* **1981,** *52* (12), 7182-7190.
19. Hess, B.; Bekker, H.; Berendsen, H. J. C.; Fraaije, J. G. E. M., LINCS: A linear constraint solver for molecular simulations. *J. Comp. Chem.* **1997,** *18*, 1463-1472.
20. Manara, R. M. A.; Tomasio, S.; Khalid, S., The Nucleotide Capture Region of Alpha Hemolysin: Insights into Nanopore Design for DNA Sequencing from Molecular Dynamics Simulations. *Nanomaterials-Basel* **2015,** *5* (1), 144-153.
21. Bhattacharya, S.; Derrington, I. M.; Pavlenok, M.; Niederweis, M.; Gundlach, J. H.; Aksimentiev, A., Molecular dynamics study of MspA arginine mutants predicts slow DNA translocations and ion current blockades indicative of DNA sequence. *ACS nano* **2012,** *6* (8), 6960-8.
22. Smart, O. S.; Neduvelil, J. G.; Wang, X.; Wallace, B. A.; Sansom, M. S. P., Hole: A program for the analysis of the pore dimensions of ion channel structural models. *J. Mol. Graph.* **1996,** *14*, 354-360.
23. Humphrey, W.; Dalke, A.; Schulten, K., VMD - Visual Molecular Dynamics. *J. Molec. Graph.* **1996,** *14*, 33-38.

Table of Contents artwork